



Multi-criteria optimization of an experimental system for the production of domestic hot water

Arnaud Lapertot, Guillaume Segond, Thomas Fasquelle, Benjamin Kadoch, Olivier Le Métayer

► To cite this version:

Arnaud Lapertot, Guillaume Segond, Thomas Fasquelle, Benjamin Kadoch, Olivier Le Métayer. Multi-criteria optimization of an experimental system for the production of domestic hot water. *Energy Conversion and Management*, 2022, 267, pp.115875. <10.1016/j.enconman.2022.115875>. <hal-03820260>

HAL Id: hal-03820260

<https://hal.science/hal-03820260v1>

Submitted on 22 Jul 2024

HAL is a multi-disciplinary open access archive for the deposit and dissemination of scientific research documents, whether they are published or not. The documents may come from teaching and research institutions in France or abroad, or from public or private research centers.

L'archive ouverte pluridisciplinaire **HAL**, est destinée au dépôt et à la diffusion de documents scientifiques de niveau recherche, publiés ou non, émanant des établissements d'enseignement et de recherche français ou étrangers, des laboratoires publics ou privés.



Distributed under a Creative Commons CC BY-NC 4.0 - Attribution - Non-commercial use - International License

Multi-criteria optimization of an experimental system for the production of domestic hot water

Arnaud Lapertot^{a,*}, Guillaume Segond^a, Thomas Fasquelle^a, Benjamin Kadoch^a,
Olivier Le Metayer^a

^a*Aix Marseille University, CNRS, IUSTI UMR 7343, 13453 Marseille, France.*

5

Abstract

An experimental domestic hot water (DHW) production system, composed of a heat pump, a heat storage and a heat exchanger is considered for this study. The IUSTI laboratory test bench recovers heat from the air extracted from a collective dwelling using a heat pump. The heat is then transferred through a heat exchanger towards a thermal storage for DHW needs. A simplified model, validated experimentally, is used to simulate the energy system. Then, a multi-criteria optimization is applied with genetic algorithms to optimize regulation and design parameters and more particularly the influence of the DHW demand profile. The objectives are to maximize the coefficient of performance and to minimize the auxiliary electrical energy. The solutions obtained must take into account constraints of the test bench and the optimization problem. Finally, a sensitivity study, based on factorial plans, is achieved to determine the set of parameters that has the strongest degradation on the objectives from the optimized solution. The optimization methodology is validated and leads to a significant improvement of the system effectiveness. Indeed, the optimal solution from the test has a gain on the coefficient of performance of 6.9 % and on the auxiliary energy of 25.2 % compared to the reference solution.

Keywords: Domestic hot water; Energy system; heat exchanger; Heat pump; Multi-objective optimization; Sensitivity study; Thermal storage.

*Corresponding author

Email address: Arnaud.Lapertot@univ-amu.fr (Arnaud Lapertot)

10 Nomenclature

Latin Symbols		Units		
			<i>cond</i>	condenser
			<i>cons</i>	consumed
	A	surface	m^2	
	c	specific heat	$J.kg^{-1}.K^{-1}$	<i>desired</i> desired water
15	E	energy	J	<i>ent</i> enthalpy
	f^*	dimensionless factor	—	45 <i>evap</i> evaporator
	H	height	m	<i>exp</i> experimental
	\dot{m}	mass flow rate	$kg.s^{-1}$	<i>in</i> input
	\dot{q}_v	volume flow rate	$m^3.s^{-1}$	<i>max</i> maximum
20	Q	thermal power	W	<i>min</i> minimum
	S	solution	—	50 <i>num</i> numerical
	T	temperature	$^{\circ}C$	<i>opt</i> optimum
	t	time	s	<i>out</i> output
	u	uncertainty	—	<i>ref</i> reference
25	V	volume	m^3	<i>thermo</i> thermocline
	W	electrical power	W	55 <i>tot</i> total
	X	parameter	—	Abbreviations
	Y	objective	—	<i>AHU</i> Air Handling Unit
	Z	position	m	<i>COP</i> Coefficient Of Performance
30	Greek symbols			<i>DHW</i> Domestic Hot Water
	α	relative deviation	%	60 <i>DHWPS</i> Domestic Hot Water Production System
	Δh	activation delay	h	<i>EACS</i> Extracted Air Conditioning System
	ϵ	effectiveness	—	<i>HP</i> Heat Pump
	ϕ	flux	W	<i>HX</i> Heat Exchanger
35	ρ	density	$kg.m^{-3}$	65 <i>NSGA</i> Non Dominated Sorting Genetic Algorithm
	σ	variation factor	%	<i>NWCS</i> Network Water Conditioning System
	Subscripts and superscripts			<i>PV</i> Photovoltaic
	<i>aux</i>	auxiliary		<i>TOPSIS</i> Technique for Order of Preference by Similarity to Ideal
	<i>circ</i>	circulator	70	
40	<i>comp</i>	compressor		<i>WWHX</i> Water-Water Heat Exchanger

1. Introduction

The energy consumption is increasing rapidly, particularly in the residential sector where it represents 21 % of total energy consumption of the world [1]. Domestic Hot Water (DHW) accounts
75 for about 20 % of energy consumption in the building sector [2] and this value will become more important with the highly insulated passive buildings. It is therefore required to increase the performance of the DHW heaters and reduces the DHW consumption while preserving constraints imposed by the rules. For example, the thermal treatment to prevent legionella appearance is carried out by heating the storage and the pipes of the distribution network [3]. Moreover, the
80 circulation of the hot water in the distribution network allows to improve user comfort by reducing the hot water arrival time [4]. The DHW requirements can be very different for each user during a day, so the variation of the DHW demand profile has a great influence in DHW production systems. Indeed, Ulrike and al. [5] have demonstrated that the influence of the DHW demand profile should not be neglected, as the energy fraction can vary up to 3 %. Furthermore, Araya
85 and al. [6] have considered six different DHW profiles, the results show a maximum deviation of 9.96 % on their cost function. Therefore, it is of interest to have relevant tools to advise the user on his DHW consumption in order to improve the performance of the system, i.e. from a user's point of view to reduce the energy consumption and thus the overall operating costs. For example, in electricity, the consumer can use the power during off-peak hours to pay less [7]. In
90 order to meet the DHW requirements, it is necessary to improve the systems dedicated to DHW production. One possible solution is the use of a production system based on a Heat Pump (HP) [8]. To compensate the higher initial investment, the energy effectiveness and reliability of such systems must be more competitive than conventional DHW systems.

In the case of a domestic hot water production system for a building, the traditional electric water
95 heater has a coefficient of performance (COP) very small of about 0.7 [9], that's why the Agency for Ecological Transition ADEME in 2015 [10] has realized a call for projects to develop innovative solutions to have COP close to 4. Moreover, a solar water heater based on solar thermal collectors

can also produce domestic hot water for a building. Indeed, Launay and al. [11] have studied the optimization of such system and they have showed that the solar fraction is high with values in the range $[0.9; 1]$. Furthermore, the thermodynamic water heater is another system that allows to satisfy the needs of heating and DHW thanks to a heat pump and a heat storage. It recovers the heat from the air to heat the water in the tank. Then electrical energy is consumed to produce a larger amount of thermal energy. Its effectiveness is expressed by the *COP* which is the ratio between the heat supplied and the power consumed. Hepbasli and al. [8] have done a review of thermodynamic water heaters and shows that the *COP* values are typically in the range of 2.0 and 3.5. By coupling the HP with a solar thermal collector, Lu and al. [12] have shown that *COP* between 2 and 6 can be reached depending on the climate conditions. Indeed, when the temperature difference between source and sink ΔT increases, the *COP* decreases. By powering the HP with photovoltaic (PV), Aguilar and al. [13] showed that the system is able to produce 130 liters of DHW at $55\text{ }^{\circ}\text{C}$, which represents 6.2 kWh in one day. The average annual *COP* of the whole system is close to 9 with a solar energy contribution of 60 %. Indeed, the PV collectors reduce the electricity consumption from the grid which allows to have much larger *COP* values. A multi-criteria optimization and decision-making procedure is used to identify the best compromise between the objectives [14]. The sizing or the regulation parameters that can control the heat pump are the volume of the DHW storage [11] or a temperature difference [15]. The influence of the DHW demand profile is also an important input variable [16]. The objectives that quantify the performance of the energy systems, are for example the *COP* [8], the cost of the system [17] or the solar fraction [13]. The optimization procedure can be carried out using genetic algorithms [18] or particle swarm algorithms [19]. Moreover, a sensitivity study is applied experimentally to determine the impact of parameter degradation on the objectives. For example, the sensitivity process can either use a method that varies one parameter at a time [15] or a factorial plan that takes into account the interactions between the parameters [11]. In addition, Atasoy and al. [20] have applied an optimization procedure to an experimental system based on heat pump integrated

water heater for household appliances. The system allows to heat 4 liters of hot water at 50 °C.

125 The optimization procedure results in an average coefficient of performance between 3 and 7.5 and leads to a 17 % decrease in energy consumption. In our study, the first difference with the literature is that the heat pump uses the energy of the air extracted from a collective building to produce domestic hot water. The second difference is the application of a multi-objective optimization procedure to determine the best regulation of the HP and the DHW demand profile.

130 The third difference is the use of an experimental plan to verify the results of the procedure.

In this study, a multi-objective optimization is performed on a domestic hot water production system composed of a heat pump and a heat storage. First of all, section 2 presents the description of the experimental bench developed in the IUSTI laboratory and the experimental protocol. Then, a simplified model that has been previously validated with the test bench is applied to dynamically

135 simulate the system. The modeling is described in section 3. Then, a multi-criteria optimization procedure is used to select the best compromise. In addition, the system's experimental bench validates the optimization procedure by carrying out tests for the reference and optimized case. This optimization methodology is presented in section 4. Finally, a sensitivity study with the factorial plan, determines the set of parameters that allows to have the strongest degradation of

140 the objectives from optimum solution. The experimental solutions of the factorial plan are also compared by computing the relative deviations from the model. The sensitivity study is described in section 5.

2. Description of the experimental set-up

2.1. Presentation of the test bench

145 The test bench of the IUSTI laboratory, illustrated in figure 1, has been developed in [15]. This experimental system allows to stock and to supply DHW using a heat pump and a thermal storage, but in this case, the system is based on the extracted air of a collective building. The set-up is composed of a recovery of extracted air, an Extracted Air Conditioning System (EACS) which

allows to regulate the temperature and the flow rate of the extracted air, and a Network Water
 150 Conditioning System (NWCS) which controls the temperature of the network water. The set-up
 also includes a Domestic Hot Water Production System (DHWPS), which is the main part of the
 experimental bench that allows to produce DHW respecting an imposed DHW demand profile.
 The test bench is not sensitive to the weather conditions because the boundary conditions (tem-
 perature, flow rate) are controlled with EACS and NWCS and set constant. The objective of the
 155 experimental procedure will be to validate the optimization procedure by performing the tests for
 the same boundary conditions.

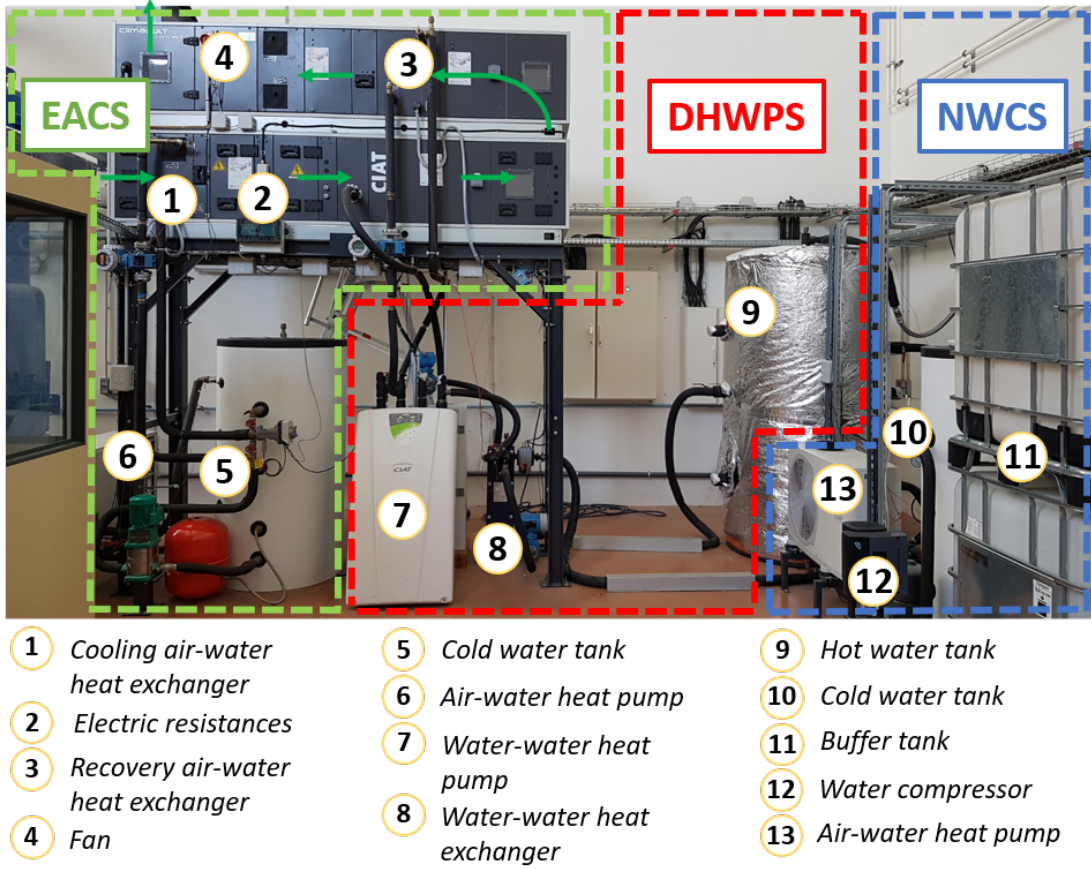


Figure 1: Picture of the DHW production test bench.

Firstly, the EACS group is used to control the temperature and the flow rate of the extracted air.

It is composed of a two-stage Air Handling Unit (AHU) in which the air is aspirated in the lower part and is rejected in the upper part (see the direction of the arrows in figure 2). The air handling unit consists of a cooling air-water heat exchanger (HX) ①, two electric resistances ②, a recovery air-water heat exchanger ③ and a fan ④. The tank ⑤ supplying the cold water is cooled using an air-water heat pump ⑥ which is connected to the AHU's cooling air-water HX. In this case, the outside air is first cooled with the HX ① and then reheated with the electric resistances ② to set the inlet temperature of the HX ③.

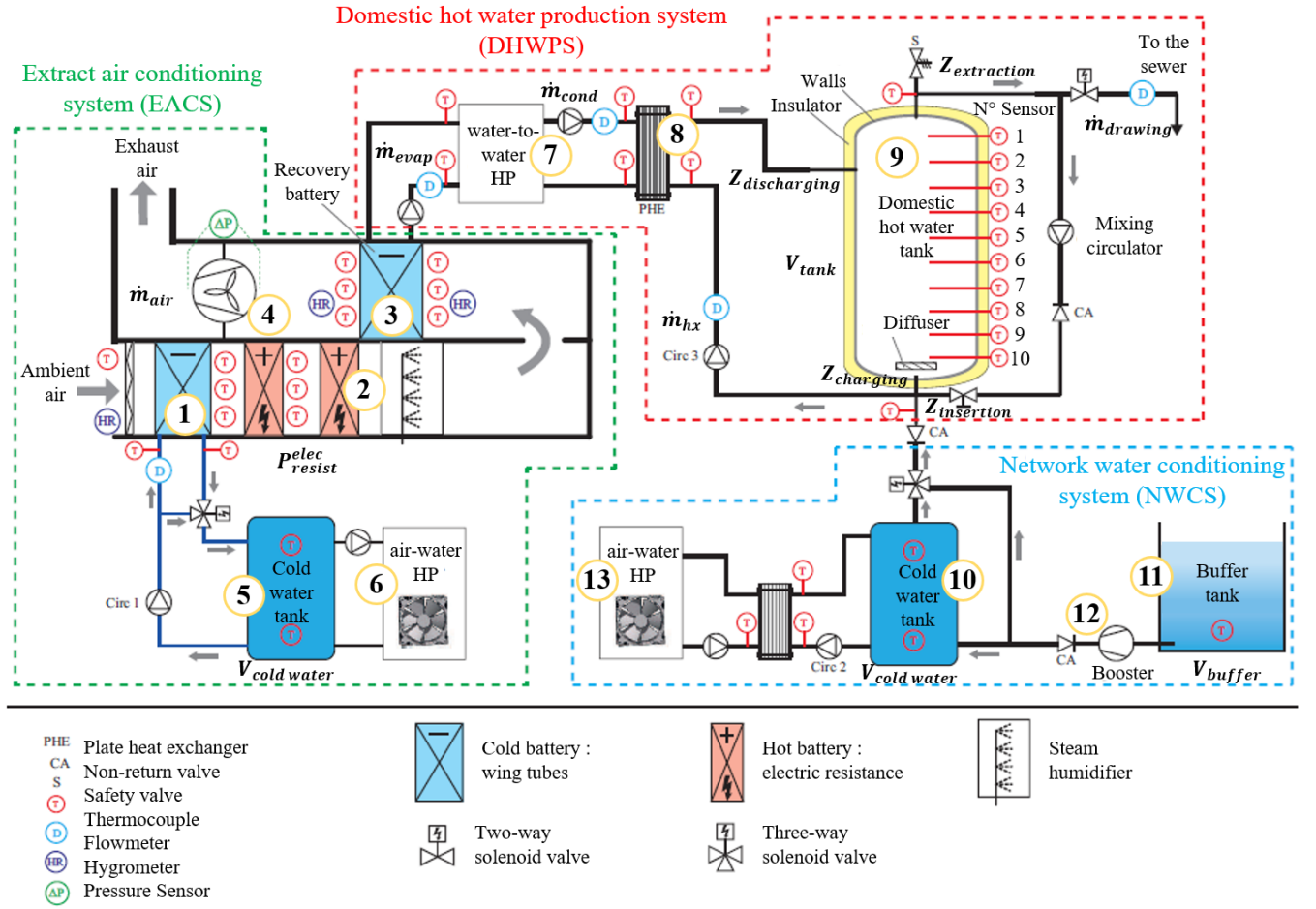


Figure 2: Scheme of the complete DHW production system [15].

Then, the NWCS group regulates the temperature of the network water, by cooling or heating

it with a reversible air/water HP and a buffer tank. Indeed, the cold water tank ⑩ is cooled using an air-water heat pump ⑬. Two water tanks ⑪ are used as a buffer zones, and a water compressor ⑫ pressurizes the water circuit and allows its circulation to the storage. A solenoid valve mixes the water in the cold water tank ⑩ with the water in the buffer tank ⑪ to set the inlet temperature of the storage tank ⑨.

Finally, the DHWPS group supplies the hot water in order to satisfy DHW demand. In fact, the air-water HX ③ recovers energy from the air in the AHU and transfers it to the water-water heat pump ⑦. This HP heats the hot water tank ⑨ through a water-water plate heat exchanger ⑧ (which role is to protect the user from potential contamination of the water by the working fluid of the HP). A solenoid valve is used to impose the drawing flow rate and therefore to extract the hot water with a typical profile.

The system also contains fan, solenoid valves, circulators, illustrated by the complete system diagram shown in figure 2. The fan is controlled with a PID module to obtain the air flow rate, the same procedure is applied with solenoid valves for the drawing flow rate. The set-up is composed of flowmeters, temperature sensors and a wattmeter. In fact, Pt100 temperature sensors are used to measure the air temperature in the AHU and ten thermocouples are used to supervise the temperature evolution within the hot water tank. A wattmeter measures the power of the heat pump compressor.

In addition, table 1 presents a summary of the dimensions of the experimental set-up. The charging and discharging positions correspond to the connection of the heat pump. They are also imposed by the test bench and the associated values are 0 m and $Z_{discharging} = 0.995\ m$. The injection position of the water from the network and the extraction position of the DHW demand are fixed at 0 m and H_{tank} .

Names	Abbreviations	Values	Units
Volume flow rate of the fan	\dot{q}_{vair}	0-3000	m^3/h
Temperature of the extracted air	T_{air}^{in}	10-30	$^{\circ}C$
Volume flow rate of water circulators	\dot{q}_{vwater}	0-3	m^3/h
Temperature of the network cold water	$T_{drawing}$	10-30	$^{\circ}C$
Desired temperature	$T_{desired}$	50-53	$^{\circ}C$
Power of the electrical heaters	$W_{resistance}$	7.8	kW
Cold water volume tank	$V_{coldwater}$	0.5	m^3
Buffer volume tank	V_{buffer}	1	m^3
Effectiveness of the air-water exchanger	$\epsilon_{air/water}$	0.7	—
Effectiveness of the water-water exchanger	$\epsilon_{water/water}$	0.83	—
Charging position	$Z_{charging}$	0	m
Discharging position	$Z_{discharging}$	0.995	m
Position of insertion of the cold water	$Z_{insertion}$	0	m
Position of domestic hot water extraction	$Z_{extraction}$	1.94	m
Internal radius of the tank	R_{tank}	0.4961	m
Internal height of the tank	H_{tank}	1.940	m
Volume of the tank	V_{tank}	1.5	m^3

Table 1: Summary of the dimensions of the experimental apparatus.

2.2. Experimental test procedure

In the following, the experimental procedure will focus on the DHWPS group, as the other groups are used to impose boundary conditions of the DHWPS. A preliminary step is to heat the hot water tank in order to have a homogeneous temperature of $T_{desired} = 53\text{ }^{\circ}C$. Moreover, the cold water tanks must be cooled to a value of $T_{drawing} = 13\text{ }^{\circ}C$ for the network water and $T_{air}^{in} = 20\text{ }^{\circ}C$ for the extracted air. The experimental tests are performed over a full day. The DHW demand profile can be started at any time of the day, but it corresponds to a simulated time $t = 5\text{ h}$. Moreover, at a simulated time $t = 21\text{ h}$, the HP is turned on in all cases in order to completely recharge the DHW tank for the next day. At the end, the experimental test is stopped at $t = 24\text{ h}$ by deactivating all components and the experimental data are retrieved using an automate memory which is connected to a computer. The experimental data generated have a time step of 10 seconds, which allows to perform energy balances to compute the objective functions that are defined in section 3.2.

The uncertainty allows to quantify the imprecision on the measurement of a quantity and it also characterizes the dispersion of the values. It gives a reliability of the results [21].

Table 2 combines the uncertainty values of the different quantities measured. The variables c and ρ are assumed to be constant with uncertainties of $6 \text{ J.kg}^{-1}.K^{-1}$ and 12 kg.m^{-3} . The values related to temperature and flow sensors are given by the manufacturers. Indeed, Pt100 have a lower uncertainty than thermocouples and the uncertainty on the flow rate is equal to 0.5 % of the value.

Quantity	Uncertainty	Unit
$u(c)$	6	$\text{J.kg}^{-1}.K^{-1}$
$u(\rho)$	12	kg.m^{-3}
$u(Pt100)$	0.54	$^{\circ}C$
$u(T_{thermocouple})$	0.71	$^{\circ}C$
$u(\dot{q}_v)$	$0.005 * \dot{q}_v$	$\text{m}^3.h^{-1}$

Table 2: Summary of uncertainty values [15]

The uncertainties on the thermal power, the coefficient of performance and on the auxiliary energy were estimated from measurements ones and with propagation of uncertainty. Consider Y is a function that depends on several variables X such that $Y(X_1, X_2, \dots, X_n)$.

$$u^2(Y) = \sum_{i=1}^n \left(\frac{\partial Y}{\partial X_i} \right)^2 u^2(X_i) \quad (1)$$

The uncertainties will be estimated to determine the reliability of the objective functions and for the graphical representation with the error bars.

3. Description of the model

3.1. System modeling

The modeling of the energy system is based on the works of [15]. The model simulates the main components of the system, *i.e.* the air-water HX, the HP, the water-water HX and the hot water

220 tank, illustrated by figure 3. The main differences between the model and the experimental bench are the following:

1. pipes are not taken into account in the model;
2. the thermocline tank is modeled with a "two-volume" assumption;
3. a speculative PV panel is powering the HP in the model.

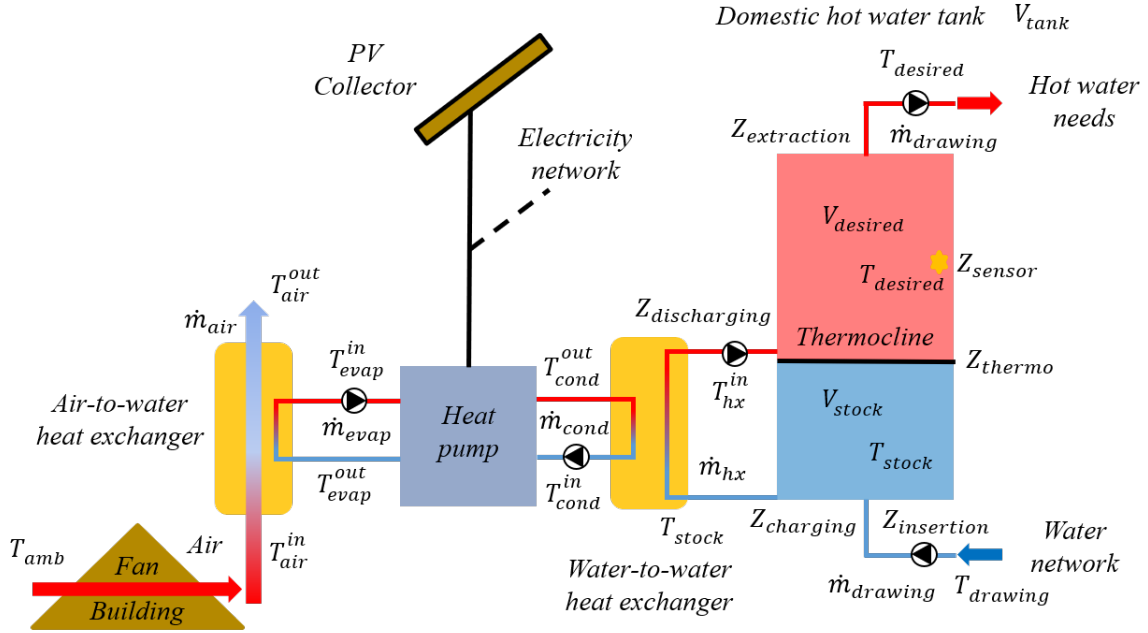


Figure 3: Scheme of the DHW production system.

225 3.1.1. Air-water heat exchanger

In the air-water HX, the inlet air temperature T_{air}^{in} and the mass flow rate \dot{m}_{air} are supposed to be known. The inlet temperature of the evaporator T_{evap}^{in} is determined from the outlet temperature of the evaporator, the inlet temperature of the air and the effectiveness of the heat exchanger $\epsilon_{air/water}$.

$$T_{evap}^{in} = T_{evap}^{out} - \epsilon_{air/water} \cdot \frac{\dot{m}_{air} c_{air}}{\dot{m}_{evap} c_{water}} \cdot (T_{evap}^{out} - T_{air}^{in}) \quad (2)$$

with \dot{m}_{evap} the mass flow rates of water. c_{air} and c_{water} correspond to the specific heat of air and water, respectively.

3.1.2. Water-to-water exchanger

The modeling of the water-water HX is similar to the air-water HX. Indeed, the calculation of the exchanger effectiveness $\epsilon_{water/water}$ allows to determine the inlet temperature of the condenser T_{cond}^{in} from the temperature of the DHW storage.

$$T_{cond}^{in} = T_{cond}^{out} - \epsilon_{water/water} \cdot \frac{\dot{m}_{hx} c_{water}}{\dot{m}_{cond} c_{water}} \cdot (T_{cond}^{out} - T_{stock}) \quad (3)$$

3.1.3. Water-to-water heat pump

The power consumed by the compressor W_{comp} and the power produced by the condenser Q_{cond} of the HP have been linked to the source and sink temperatures thanks to various experiments from the test bench that ended in robust correlations.

$$\begin{cases} Q_{cond} &= f_1(T_{evap}^{in}, T_{cond}^{in}) \\ W_{comp} &= f_2(T_{evap}^{in}, T_{cond}^{in}) \end{cases} \quad (4)$$

A heat balance on the HP determines the evaporation power, assuming no heat losses to the environment:

$$Q_{evap} = Q_{cond} - W_{comp} \quad (5)$$

The expression of functions f_1 and f_2 was obtained by ordinary least squares regression using a third-order polynomial with two variables, based on experimental results:

$$\begin{aligned} Q = & C_1 + C_2 T_{evap} + C_3 T_{cond} + C_4 T_{evap}^2 + C_5 T_{evap} T_{cond} + C_6 T_{cond}^2 \\ & + C_7 T_{evap}^3 + C_8 T_{cond} T_{evap}^2 + C_9 T_{evap} T_{cond}^2 + C_{10} T_{cond}^3 \end{aligned} \quad (6)$$

with C_1, \dots, C_{10} the values of the coefficients which are different for the functions f_1 and f_2 , as

indicated in table 3. The outlet fluid temperatures of the evaporator and the condenser are then obtained from the following equations:

$$\begin{cases} T_{evap}^{out} = T_{evap}^{in} - \frac{Q_{evap}}{\dot{m}_{evap} c_{water}} \\ T_{cond}^{out} = T_{cond}^{in} + \frac{Q_{cond}}{\dot{m}_{cond} c_{water}} \end{cases} \quad (7)$$

230 The water outlet of the evaporator correspond to the inlet of the air/water HX and the water outlet of the condenser is the inlet of the water/water HX.

Coefficient	W_{comp}	Q_{cond}
C_1	$6.303 * 10^{-1}$	$5.301 * 10^0$
C_2	$2.696 * 10^{-2}$	$3.738 * 10^{-1}$
C_3	$7.586 * 10^{-3}$	$-4.368 * 10^{-2}$
C_4	$-1.919 * 10^{-3}$	$-1.013 * 10^{-2}$
C_5	$2.874 * 10^{-4}$	$1.136 * 10^{-3}$
C_6	$3.153 * 10^{-4}$	$2.429 * 10^{-4}$
C_7	$3.536 * 10^{-5}$	$1.825 * 10^{-4}$
C_8	$7.849 * 10^{-6}$	$-1.202 * 10^{-5}$
C_9	$-8.923 * 10^{-6}$	$-2.053 * 10^{-5}$
C_{10}	$1.688 * 10^{-6}$	$-1.335 * 10^{-6}$

Table 3: Summary of the different coefficients for the HP modeling.

3.1.4. Domestic hot water tank

The tank is modeled, assuming an infinitely thin thermocline separating the volume into two parts. Indeed, the upper part assumed to contain water at the desired temperature $T_{desired}$. The lower part has a variable temperature T_{stock} which is calculated for each time step from an energy balance. This equation is composed of a time variation that expresses the energy storage in the tank, an enthalpic term which increases the temperature of the storage when the heat pump is working and a DHW demand term which decreases this temperature. The evolution of the storage temperature T_{stock} is given by the following formula:

$$\rho_{water} c_{water} V_{stock}(t) \frac{\partial T_{stock}}{\partial t} = \phi_{ent_{hx}} - \phi_{drawing} \quad (8)$$

with ρ_{water} the density of water and V_{stock} the volume of storage in the lower part. The heat transferred in the tank $\phi_{ent_{hx}}$ is determined from an enthalpy balance of the water between the DHW tank and the water-water HX.

$$\phi_{ent_{hx}} = \dot{m}_{hx} c_{water} (T_{hx}^{in} - T_{stock}) \quad (9)$$

where T_{hx}^{in} is the temperature of the hot water which entering the DHW tank. It is defined by:

$$T_{hx}^{in} = T_{stock} - \epsilon_{water/water} \cdot \frac{\dot{m}_{hx} c_{water}}{\dot{m}_{cond} c_{water}} \cdot (T_{stock} - T_{cond}^{in}) \quad (10)$$

The hot water drawing flux is a function of a DHW user profile, the network temperature and the storage temperature. This power is only used in the lower part of the thermocline, in fact, when the DHW demand is carried out, the volume V_{stock} increases as a function of the drawing flow rate $\dot{m}_{drawing}$ and the temperature T_{stock} decreases, because the network water $T_{drawing}$ is colder.

$$\phi_{drawing} = \dot{m}_{drawing} c_{water} (T_{stock} - T_{drawing}) \quad (11)$$

The variation of the volume in the lower part of the tank is obtained from a profile $\dot{m}_{drawing}$. The mass conservation equation is expressed by:

$$\rho_{water} \frac{\partial V_{stock}}{\partial t} = \dot{m}_{drawing} - \dot{m}_{hx} \quad (12)$$

The volume of the upper part is obtained from the volume of the lower part and the total volume of the tank. Moreover, if the temperature of the lower part reaches the desired temperature, then the volume of the lower part is set to 0 and the stock is considered to be full. Furthermore, the

positions of the thermocline Z_{thermo} and its dimensionless value Z_{thermo}^* are determined by:

$$Z_{thermo}^* = \frac{Z_{thermo}}{H_{tank}} \quad \text{with} \quad Z_{thermo} = \frac{V_{stock}}{A_{tank}} \quad (13)$$

The storage model also takes into account stratification with two temperatures by identifying the temperature in each sensor. The tank is monitored by 10 sensors whose positions are indicated by the values of Z_i , as illustrated in Figure 4 (left). For each sensor, the model checks if the position of thermocline is lower than that of the sensors. If this is the case in this case, the temperatures T_i are equal to $T_{desired}$ otherwise to T_{stock} .

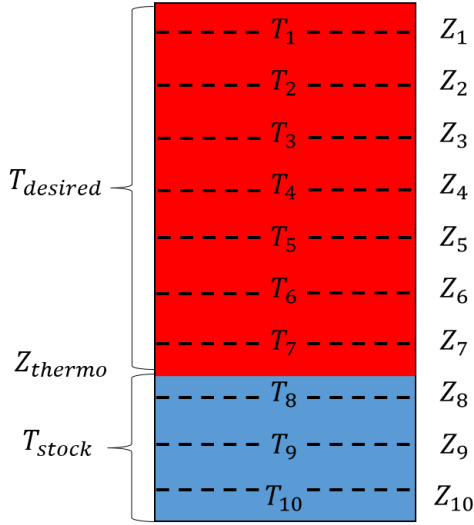


Figure 4: Scheme of the thermocline model.

N° sensor	Z_{sensor}	Z_{sensor}^*
Units	m	—
1	1.825	0.941
2	1.635	0.843
3	1.445	0.745
4	1.255	0.647
5	1.065	0.549
6	0.875	0.451
7	0.685	0.353
8	0.495	0.255
9	0.305	0.157
10	0.115	0.059

Table 4: Position of the sensors in the DHW storage tank.

3.1.5. Weighted average temperature submodel of the DHW storage tank

The addition of a DHW storage submodel is important to integrate the mixing condition between hot and cold water volumes below the discharging position. Indeed, if the thermocline position Z_{thermo} is lower than the discharging position $Z_{discharging}$ when the heat pump is switched on, then a weighted average temperature submodel should be used to re-compute the storage temperature, illustrated by figure 5.

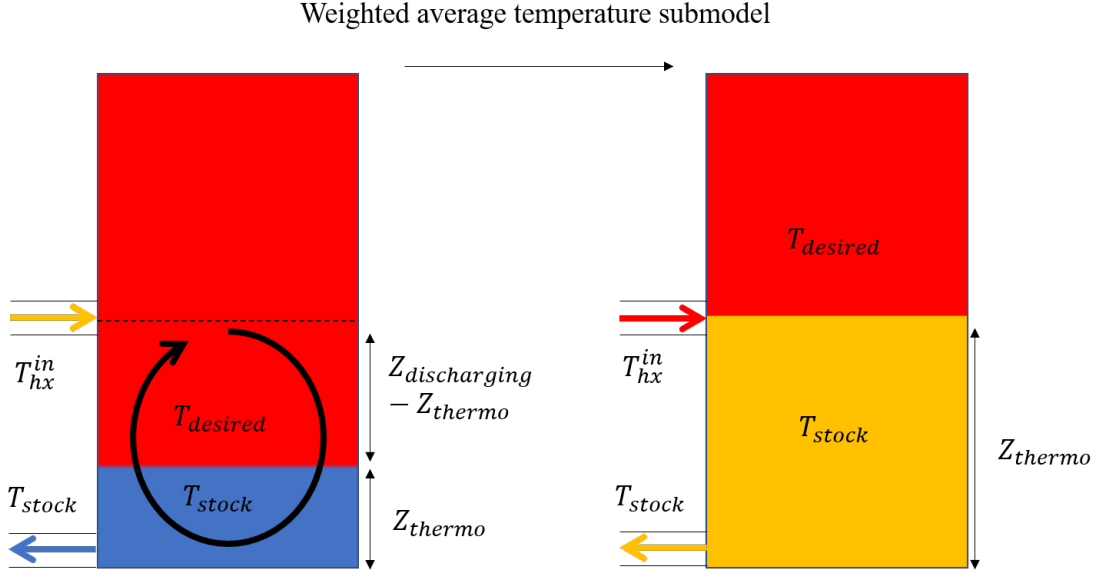


Figure 5: Sketch of the weighted average temperature submodel.

It is the average of the storage temperature weighted at the thermocline position and the desired temperature weighted at the discharging position. The thermocline position is then forced to the discharging position.

$$\begin{cases} T_{stock}(t) = \frac{Z_{thermo}(t) T_{stock}(t) + (Z_{discharging} - Z_{thermo}(t)) T_{desired}}{Z_{discharging}} \\ Z_{thermo}(t) = Z_{discharging} \end{cases} \quad (14)$$

The dimensionless value of T_{stock} is expressed as follows:

$$T_{stock}^* = \frac{T_{desired} - T_{stock}}{T_{desired} - T_{drawing}} \quad (15)$$

250 The numerical time integration is based on Euler explicit scheme. The simulation time is 24 hours with a time step of 10 seconds. The simplified model has been experimentally validated by comparing experimental and numerical results for reference cases and resulting in a deviation smaller than 5 % for the various scenarios [15].

3.2. Methods description

255 The methods of multi-objective optimization, multi-criteria decision-making and sensitivity study are explained in this section by describing objectives, variables and constraints.

3.2.1. Definition of criteria, variables and constraints

The objectives of the optimization problem are to maximize the coefficient of performance COP and to minimize the auxiliary energy E_{aux} . A daily average COP for the whole system is defined
260 by calculating the ratio between the heat supplied to the DHW and the global energy consumption of the HP compressor, the circulators and the fan [15].

$$COP = \frac{\int_{0h}^{24h} \dot{m}_{drawing} c_{water} (T_{desired} - T_{drawing}) dt}{\int_{0h}^{24h} (W_{comp} + W_{circ} + W_{fan}) dt} \quad (16)$$

The whole power consumption of the fan is not taken into account because it is an essential part of the air renewing system, and therefore it is not an actual part of the heat recovery system. However, the insertion of the heat recovery HX introduces additional pressure drops that are
265 assumed to create a 200 W over-consumption of the fan. In addition, the power consumption of the circulator (that are used only when the HP is on) is 50 W [15].

The auxiliary energy corresponds to the part of energy that does not come from solar resources because the considered system can be connected to photovoltaic modules that operate hypothetically between 8 and 19 hours. The auxiliary energy E_{aux} is the difference between the consumed energy by the system and the produced energy by the PV modules.

$$E_{aux} = \int_{0h}^{24h} (W_{comp} + W_{circ} + W_{fan}) dt - \int_{8h}^{19h} W_{PV} dt \quad (17)$$

The solar collectors are dimensioned such that their produced power compensates the consumption

of the compressor, the circulators and the fan.

$$W_{PV} = W_{comp} + W_{circ} + W_{fan} \quad (18)$$

In this study, the relative deviation is used to quantify the difference between the numerical and experimental solutions, and is defined as follows:

$$\alpha = \frac{Y^{exp} - Y^{num}}{Y^{num}} \quad (19)$$

with Y^{exp} and Y^{num} the value of the experimental and numerical objectives functions, respectively. In addition, the system variables are the regulation parameters and the DHW demand shape: the HP is triggered if the thermocline position is larger than a set sensor position Z_{sensor} . The dimensionless variable Z_{sensor}^* is a function of the tank height H_{tank} .

$$Z_{sensor}^* = \frac{Z_{sensor}}{H_{tank}} \quad (20)$$

Moreover, the delay Δh is another parameter that activates the HP with a certain delay after the first peak of the DHW consumption. Furthermore, figure 6 shows the DHW demand profile over a day. It is composed of three Gaussian which represent the peaks of the domestic hot water consumption. The total DHW demand volume is set at $V_{tot} = 1.5 \text{ m}^3$, this corresponds to the daily consumption of a dozen dwellings. The cumulative demand DHW volume is defined as follows:

$$V_{tot}^* = \frac{1}{\rho_{water} * V_{tot}} \int_0^t \dot{m}_{drawing} dt \quad (21)$$

Indeed, the solenoid valve leads to volume flows with a minimum resolution of $0.1 \text{ m}^3/h$, so the DHW demand profile must be truncated (see figure 6).

The volume of the second peak is always $V_{peak2} = 10 \%$ compared to V_{tot} . The volume of the first

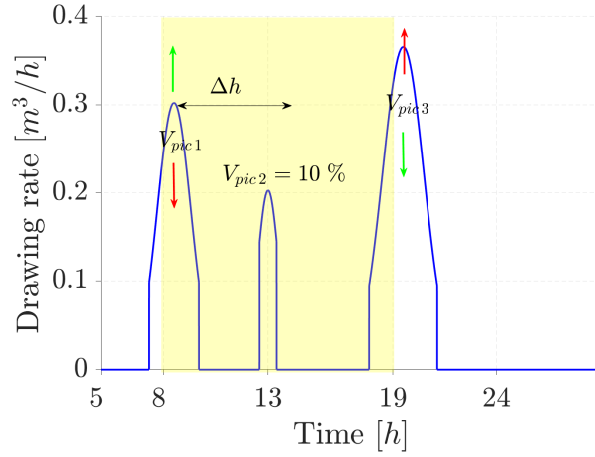


Figure 6: DHW demand profile according to the time. The yellow area indicates the operating time interval of the PV modules.

peak $V_{peak\ 1}$ is a parameter which may varies between 25 % and 75 % related to the total volume. The volume of the third peak $V_{peak\ 3}$ is defined by:

$$V_{peak\ 3} = V_{tot} - V_{peak\ 1} - V_{peak\ 2} \quad (22)$$

The DHW demand volume $V_{peak\ 1}$ represents the consumption of the first peak, and its dimensionless value $V_{peak\ 1}^*$ is determined by:

$$V_{peak\ 1}^* = \frac{V_{peak\ 1}}{V_{tot}} \quad (23)$$

270 Table 5 contains the reference values and the range limits for the different variables. The dimensionless volume of the first peak $V_{peak\ 1}^*$ and the delay Δh can take any value between their minimum and maximum, which is not the case of the dimensionless sensor position Z_{sensor}^* because of experimental constraints.

The constraints of the optimization problem must be considered to respect the rules, they must eliminate legionella and satisfy DHW's needs. Indeed, the DHW tank must be heated to 53 °C during 2 hours in order to avoid the proliferation of legionella [22]. Furthermore, to satisfy DHW's

Names	Reference	Minimum	Maximum	Units
Z_{sensor}^*	0.549	0.087	0.913	—
$V_{peak\ 1}^*$	0.35	0.25	0.75	—
Δh	6	0	12	h

Table 5: Reference parameters with limits.

needs, the tank must always contain hot water, which means that the thermocline position Z_{thermo} must never exceed the tank height H_{tank} .

$$Z_{thermo} < H_{tank} \quad (24)$$

The process must take into account experimental constraints. Indeed, the test bench tank is
 275 instrumented with ten temperature sensors whose positions are given in table 4. Therefore, Z_{sensor}^* must be discretized to respect these constraints.

3.2.2. Multi-criteria optimization

A multi-criteria optimization problem seeks to find the set of solutions that simultaneously optimize several functions. The solutions are composed of variables and objectives. The variables, also
 280 called parameters, are included in the research space. These objectives functions can also be called objectives or criteria, are included in the solutions space. The problem may be subjected to constraints that limit the research and the solution spaces. Moreover, a multi-criteria optimization procedure does not provide a unique solution compared to a mono-objective one because the objective functions are not necessarily comparable and do not evolve in the same direction. The
 285 works of Vilfredo Pareto [23] have shown that it is impossible to improve all objectives at the same time. Indeed, the improvement of one or several objectives will necessarily degrade the other objectives. The results of a multi-criteria optimization problem give a set of solutions that is a good compromise with respect to the different objectives, including the best solutions for each criterion. These results are composed of the non-dominant solutions and are gathered on a curve
 290 called the Pareto front. By definition, a solution X dominates another solution Y if and only if,

for any f_i objective, $f_i(X)$ is smaller than or equal to $f_i(Y)$ with at least one strict inequality. In addition, there are many optimization methods such as the Nelder-Mead method, the simplex technique, particle swarm algorithms and genetic algorithms [24]. Genetic algorithms are suitable for constrained multi-objective problems and for discrete and non-linear programming. These
295 algorithms are probabilistic optimization methods based on the evolution of species. They have been initially developed by the works of John Holland [25]. Based on the processes of selection, crossing and mutation, individuals evolve over generations in order to survive in their natural environment.

In this study, the NSGA-II algorithm [26] are applied with a mutation and crossing percentage
300 equal to 50 %. The number of individuals and the number of generations are 100 and 1000, respectively.

3.2.3. Multi-criteria decision-making applied to optimization

The decision aid is a technique that selects the best compromise among Pareto's solutions. There are a large number of multi-criteria decision-making methods. The weighted sum method and the
305 Technique for Order of Preference by Similarity to Ideal Solution (TOPSIS) method are the most used and known [27]. The TOPSIS is the most appropriate for this kind of system and consists in selecting the solution that has the closest distance to the ideal solution.

The procedure of the TOPSIS method [27] is , firstly, to normalize the objectives.

$$r_j = \frac{|f_j - \min(f_j)|}{|\max(f_j) - \min(f_j)|} \quad (25)$$

Then, the function v is defined by taking into account the normalized function r and the weight w of each criterion which quantifies the relative importance of the criteria.

$$v_j = w_j r_j \quad (26)$$

The positive ideal solution PIS and the negative ideal solution NIS are defined from the minimum or maximum of the function v depending on whether the objective j belongs to the set C^+ or C^- . If the objective j seeks a maximum, so it belongs to the set C^+ and reciprocally for C^- .

$$\begin{cases} PIS_j = [\max(v_j) \mid j \in C^+, \min(v_j) \mid j \in C^-] \\ NIS_j = [\min(v_j) \mid j \in C^+, \max(v_j) \mid j \in C^-] \end{cases}$$

Moreover, the distances D^+ and D^- are calculated from the following Euclidean norm:

$$\begin{cases} D^+ = \sqrt{\sum_{j=1}^m [v_j - PIS_j]^2} \\ D^- = \sqrt{\sum_{j=1}^m [v_j - NIS_j]^2} \end{cases}$$

with m the number of objectives. Finally, the best compromise is obtained by:

$$S = \max \left(\frac{D^-}{D^+ + D^-} \right) \quad (27)$$

In this study, the best solution selected by the TOPSIS method is called the best compromise or the optimal solution. The ideal solution corresponds to the maximum of the COP and the minimum of the E_{aux} . The weight associated with each criterion is 1/2.

3.2.4. Sensitivity study

The sensitivity analysis is the study of how the uncertainty in the output of a system can be attributed to the uncertainty in its inputs [28]. Its goal is to identify and to classify the most influential inputs, to map the behaviour of the outputs in relation to the inputs.

In this study, the sensitivity study is used to check if the solution selected by the previous methods corresponds to the optimal solution. For this purpose, two-level factorial plans require 2^k eval-

uations with $k = 3$ the number of parameters [29]. This method requires few evaluations and provides information on the interaction of the parameters. The procedure for factorial plans is explained in [11].

3.2.5. Multi-criteria decision-making applied to sensitivity study

The TOPSIS method is also used to select the solution that strongly degrades the objectives functions among the factorial plans solutions. The weight associated with each criterion is set at 1/2. However, the selected alternative must be the furthest from the best compromise to have the largest degradation with respect to the optimal solution.

In this part, the worst solution is determined using the TOPSIS method with the following expression:

$$S = \min \left(\frac{D^-}{D^+ + D^-} \right) \quad (28)$$

4. Multi-criteria optimization procedure

In this study, the optimization methodology is performed in three steps. Firstly, the NSGA-II multi-objective optimization algorithm provides the Pareto front. Secondly, the TOPSIS multi-criteria decision-making method selects the optimal solution. Thirdly, the solution obtained by the multi-objective optimization is realized experimentally.

4.1. Simulation of the reference case

The chosen values of the reference case is introduced in table 5. The heat pump regulation makes it possible to heat the hot water tank if the parameter Δh exceeds 6 hours after the first peak of DHW consumption or if the thermocline position is higher than 1.07 m in the storage tank. The first, the second and the third volume peaks are respectively 35 %, 10 % and 55 % of the total volume. In all cases, the heat pump is activated at 21 h, so that the tank is charged the next day.

The system under consideration is connected to PV panels that allow the heat pump to operate between 8 and 19 hours (yellow zone).

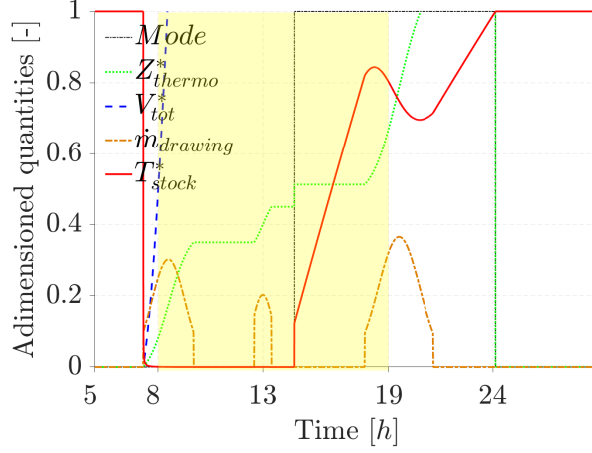


Figure 7: Dynamics of the reference case. The yellow area indicates the operating time interval of the PV modules. The orange and blue curves correspond to the instantaneous and cumulative DHW demand profiles. The black, red and green curves represent the HP operating mode, the storage tank temperature and the thermocline position respectively. T_{stock}^* and V_{tot}^* correspond to the dimensionless values of the storage temperature and the accumulated DHW demand volume.

Figure 7 illustrates the system dynamics for the reference case over one day. The DHW demand volume increases in the same way as the thermocline position because the tank volume and the DHW demand volume are both equal to 1.5 m^3 . The temperature of the stock T_{stock}^* increases when the HP is on. The position Z_{thermo}^* is reset to 0 when the storage temperature reaches the desired temperature ($T_{stock}^* = 1$), this means that the tank is fully charged with hot water. Moreover, when the heat pump is switched on, the discharging position is higher than the thermocline position, the weighted average temperature submodel forces the thermocline to the $Z_{discharging}$ value. In this case, the storage temperature increases, because it is re-computed by averaging the desired temperature and the storage temperature below the discharging position. In addition, the daily balance illustrates that the produced energy by the HP is 69.67 kWh and the consumed energy is equal to 22.13 kWh , which gives a COP of 3.148. The produced energy by the photovoltaic collectors is 9.513 kWh and the E_{aux} is 12.62 kWh .

The heat exchanger model is validated because the relative deviations are 9.7 % and 14 % for T_{evap} and T_{cond} , respectively. The HP model is also validated because the average relative deviations are 6.5 %, 5.6 % and 6.7 % for Q_{evap} , W_{comp} , Q_{cond} , respectively. These experimental and numerical powers are compared in figure 12. The storage model (thermocline of zero thickness) with the associated the weighted average temperature submodel, is validated because the average relative deviations are very small with values of 2 – 8 % the different sensors. In addition, the coefficient of performance, which is the ratio between the energy produced on the energy consumed, gives a value 3.221 for COP^{exp} and 3.148 for COP^{num} is with a relative difference of 2.3 %. The auxiliary energy is the difference between the energy produced by the PV collectors and the electricity consumption, has a value of 11.63 *kWh* for the experimental set-up and 12.62 *kWh* for the numerical model with a relative deviation of 8.5 %. The model gives a very good estimation of the indicators (the coefficient of performance COP and the auxiliary energy E_{aux}) and a good representation of the dynamics.

Name	Unit	Experimental value	Numerical value	α
E_{fan}	kWh	4.800	4.800	0.0
E_{circ}	kWh	0.464	0.481	3.8
E_{comp}	kWh	15.89	16.85	6.0
E_{cons}	kWh	21.16	22.13	4.6
E_{prod}	kWh	68.14	69.67	2.2
$E_{prod_{PV}}$	kWh	9.530	9.513	0.2
COP	-	3.221	3.148	2.3
E_{aux}	kWh	11.63	12.62	8.5

Table 6: : Energy summary for the reference case.

4.2. Multi-objective optimization

The objectives, variables and constraints are described in section 3.2. The results of the multi-criteria optimization are gathered in two parts: the maps and the Pareto front.

The maps display all the solutions obtained by the genetic algorithms according to criteria and parameters. Figure 8 shows that the COP is between 2.654 and 3.472. The COP is maximum for

370 large values of Z_{sensor}^* and Δh , and for a small value of V_{peak1}^* . Indeed, the consumed energies by the circulators, the fan and the compressor vary according to the operating time of the HP.

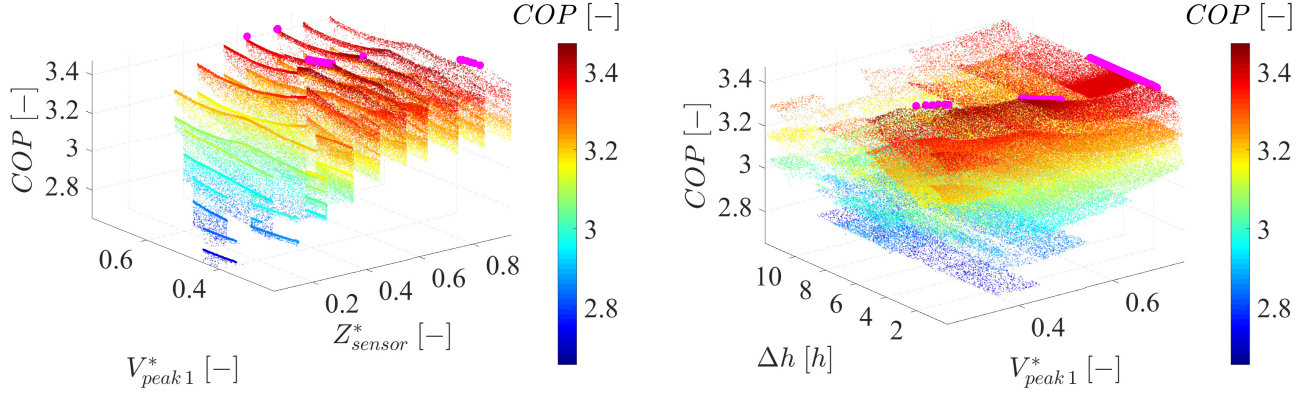


Figure 8: Mapping of the COP according to the parameters. The pink dots correspond to Pareto's solutions.

Figure 9 shows that the E_{aux} varies between 5.633 and 15.66 kWh . The auxiliary energy is maximum for a large value of Z_{sensor}^* , Δh and for a small value of V_{peak1}^* . Indeed, for these parameter values, the HP is not correctly regulated and it is activated much too late, which
 375 implies that it is not activated during the day. Furthermore, in the case where the volume of the first peak increases, the sensor position and the delay decrease, the HP is activated more quickly and the storage tank is charged during the day. Therefore the E_{aux} decreases because the consumed

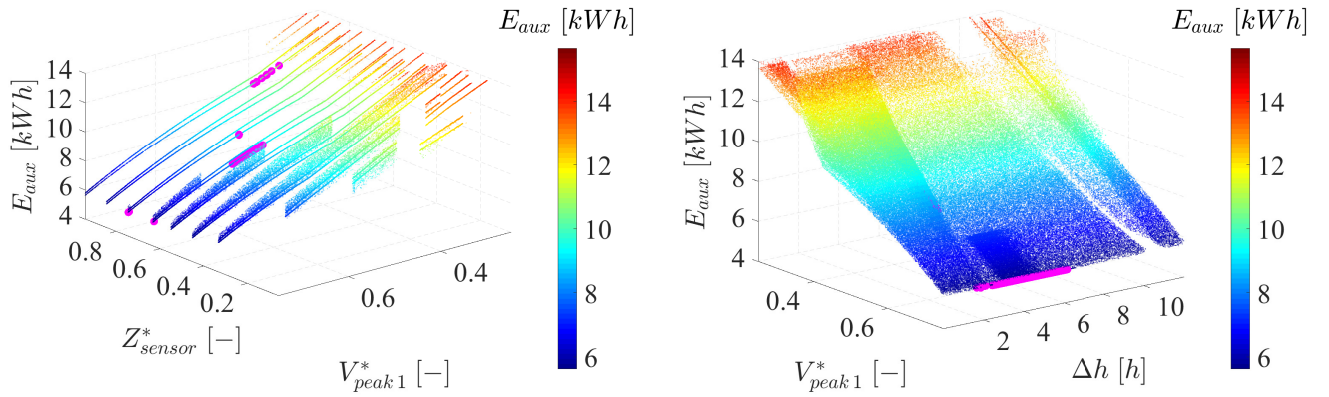


Figure 9: Mapping of the E_{aux} according to the parameters. The pink dots correspond to Pareto's solutions.

energy is supplied directly by the photovoltaic collectors.

Figure 10 a) displays the set of solutions as a function of the objectives. The good compromises are obtained by maximizing the COP and minimizing the E_{aux} . This figure identifies the Pareto front, presented by the pink dots. Figure 10 b) illustrates the Pareto solutions depending on the sensor position. The best compromises have a value of Z_{sensor}^* which varies from 0.647 to 0.941. When the COP and the E_{aux} increase, the sensor position also increases and then decreases. Indeed, the

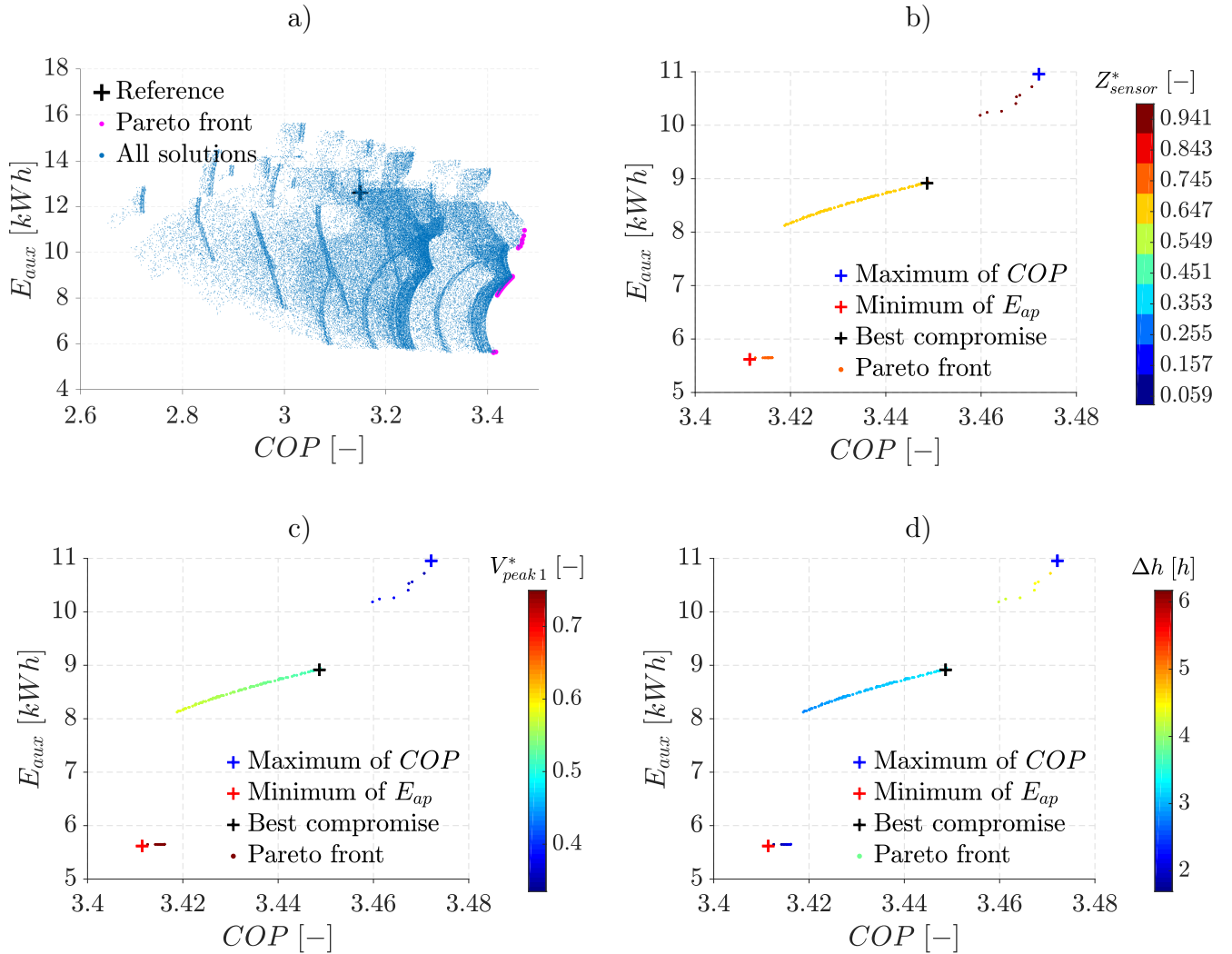


Figure 10: Representation of all the solutions according to the COP and the E_{aux} a). The pink dots correspond to the Pareto front. Graphical representation of the Pareto front as a function of Z_{sensor}^* b), V_{peak1}^* c) and Δh d).

thermocline position reaches the sensor position less quickly when Z_{sensor}^* increases. Therefore, the E_{aux} decreases because the HP is switched on for a large part of the night and the COP is stronger because the consumed energy by the HP compressor decreases as it operates less time. Then, figure 10 c) shows that V_{peak1}^* varies between 0.33 and 0.75. When the volume of the first peak of DHW consumption increases, the E_{aux} decreases because the HP is activated more quickly for a fixed sensor position. The tank heats during the day, which is in adequacy with the production of the PV collectors. Moreover, when V_{peak1}^* increases, the COP decreases because the consumed energy by the HP increases. Finally, figure 10 d) illustrates Pareto front for Δh varying from 1.7 to 6.2 hours. When the delay increases, the COP and the E_{aux} increase because the produced energy by the PV collectors is increasing and the consumed energy by the HP is decreasing. In addition, the two constraints on legionella treatment and on DHW's needs are respected for each Pareto's solutions.

4.3. Multi-criteria decision-making applied to optimization

The TOPSIS decision-making method is applied to select the solution that presents the best compromise between the COP and the E_{aux} . Table 7 provides the reference solution, the $\max(COP)$, the $\min(E_{aux})$ and the optimal solution. The criteria do not evolve in the same direction because the maximum of COP is obtained by degrading the E_{aux} and reciprocally. Moreover, the maximum of COP solution allows having a value of 3.472 with a very high E_{aux} equal to 10.95 kWh. This solution is obtained for a high sensor position and a small peak volume and delay. In addition, the minimum of E_{aux} solution is obtained with a COP of 3.407 and an E_{aux} of 5.633 kWh. The values of the sensor position and the delay are small, and the peak volume is very large. Furthermore, the best compromise obtained with the TOPSIS method has a $COP = 3.450$ and an $E_{aux} = 8.926$ kWh. The value of the parameters is 0.745 for Z_{sensor}^* , 0.513 for V_{peak1}^* and 3.322 hours for Δh .

Figure 11 compares the dynamic simulation of the reference case a), the optimized solution b),

/	Objectives			Variables	
Names	COP	E_{aux}	Z_{sensor}^*	$V_{peak\ 1}^*$	Δh
Units	—	kWh	—	—	h
<i>Ref</i>	3.148	12.62	0.549	0.350	6.000
$\max(COP)$	3.472	10.95	0.941	0.335	4.712
$\min(E_{aux})$	3.407	5.633	0.745	0.749	2.440
<i>TOPSIS</i>	3.450	8.926	0.745	0.513	3.322

Table 7: Coordinates of the reference, the maximum of COP , the minimum of E_{aux} and the best compromise obtained with TOPSIS. The bold characters indicate that the heat pump is regulated from $V_{pic\ 1}^*$ or Δh .

the maximum of COP c) and the minimum of E_{aux} d). Figures 11 b, c and d) show that the thermocline position does not reach the top of the storage tank, thus DHW demand is satisfied. In addition, the heat treatment for the legionella elimination is respected because the storage tank is heated for more than two hours at 53 °C. Indeed, figure 11 b) shows that the HP operates for a shorter time, and the E_{aux} decreases due to a better valorization of the solar resource which is in adequacy with the HP operating range. Moreover, figure 11 c) has a rather small operating time. The HP operates mostly at night, that is why the E_{aux} is large. Furthermore, figure 11 d) depicts a regulation that activates the HP mainly during the day. However, the operating time is longer so the COP is smaller.

In addition, a daily balance shows that the produced energy is the same for all solutions because the DHW demand volume is always 1.5 m^3 . For the best compromise, the consumed energy is smaller 20.19 kWh and the produced energy by the PV collectors is larger 11.27 kWh compared to the reference case. This optimization procedure significantly improves the domestic hot water system because the COP has increased and the E_{aux} has decreased compared to the reference solution.

4.4. Experimental optimization procedure

Figure 12 a), on the left, shows the DHW demand profile for the reference case. It is composed of three Gaussian curves which represent the daily consumption of DHW. This profile are truncated

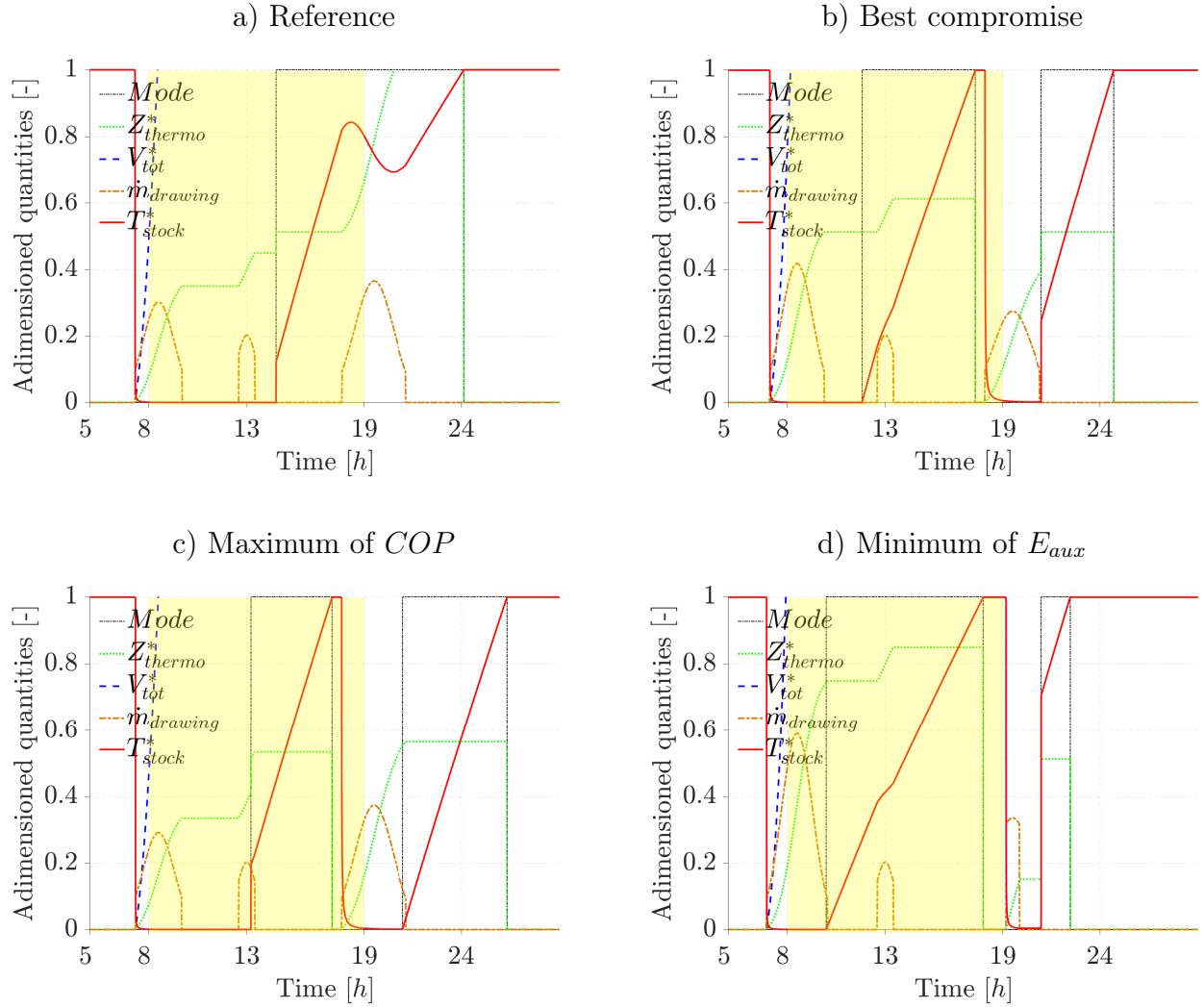


Figure 11: Dynamic simulation for different solutions. The orange and blue curves correspond to the instantaneous and cumulative DHW demand profiles. The black, red and green curves represent the HP operating mode, the storage tank temperature and the thermocline position respectively. T_{stock}^* and V_{tot}^* correspond to the dimensionless values of the storage temperature and the accumulated DHW demand volume.

to $0.1 \text{ m}^3/\text{h}$, as presented previously. The yellow square corresponds to the operating range of the photovoltaic collectors. The drawing flow rate of the test is close to the numerical one, however, the experimental curve is more fluctuating due to external conditions. The total DHW demand volume is 1.47 m^3 for the test and 1.50 m^3 for the model so the relative deviation is 2.0 %. Figure 12 b), on the left, illustrates the experimental temperature evolution for five different sensors. The temperature simulated by the model is shown by the black line. The purple, blue, green,

435 yellow and red blue curves correspond to sensors 10, 7, 5, 3 and 1, respectively. The results
 show that the global shape of the experimental curves are close to the numerical ones because
 the heat pump is switched on and off at the same time. In fact, the heat pump operates 9.33 h
 for the model compared to 9.37 h for the test so the relative difference is 5.3 %. Moreover, there
 are differences in the temperature of the intermediate sensors. In fact, the experimental profiles
 440 decrease progressively due to the stratification of the temperature in the tank. The numerical
 ones decrease suddenly because the thickness of the thermocline is zero. The profile changes from
 the desired temperature to the storage temperature when the thermocline reaches the sensors
 positions. Similarly, the initial storage temperature is not homogeneous at 53 °C but is stratified
 between 52 and 54 °C. The final temperature progressively decreases due to heat losses that are
 445 not taken into account in the thermocline model. Figure 12 c), on the left, exhibits the power
 evolution of the heat pump. The red, blue and green curves relate to the condenser, compressor
 and evaporator, respectively. During the function range of the heat pump, the condenser power
 is larger than the compressor and evaporator power, because the heat pump provides more power
 than it consumes. Moreover, when the storage temperature increases, the thermal power decreases
 450 and the electrical power increases because the compressor must provide more power to heat the
 storage tank to reach its desired temperature.

In addition, figure 12 a), on the right, shows the DHW demand profile for the optimized solution.
 The experimental and numerical results are very similar because the experimental data are super-
 imposed on the numerical data. Nevertheless, the experimental curve is more fluctuating. Figure
 455 12 b), on the right, illustrates the comparison between the temperature for the test and the model.
 The evolution of the experimental and numerical temperatures is similar because the storage tank
 starts at a temperature of 53 °C and then decreases drastically to 13 °C when the thermocline
 reaches the sensors positions. The HP is on once during the operating range of the PV collector
 and then switched off when the storage temperature reaches 53 °C. The consumption of the third
 460 peak reduces the T_{stock} and the HP is reactivated at 21 h to supply for the energy demand.

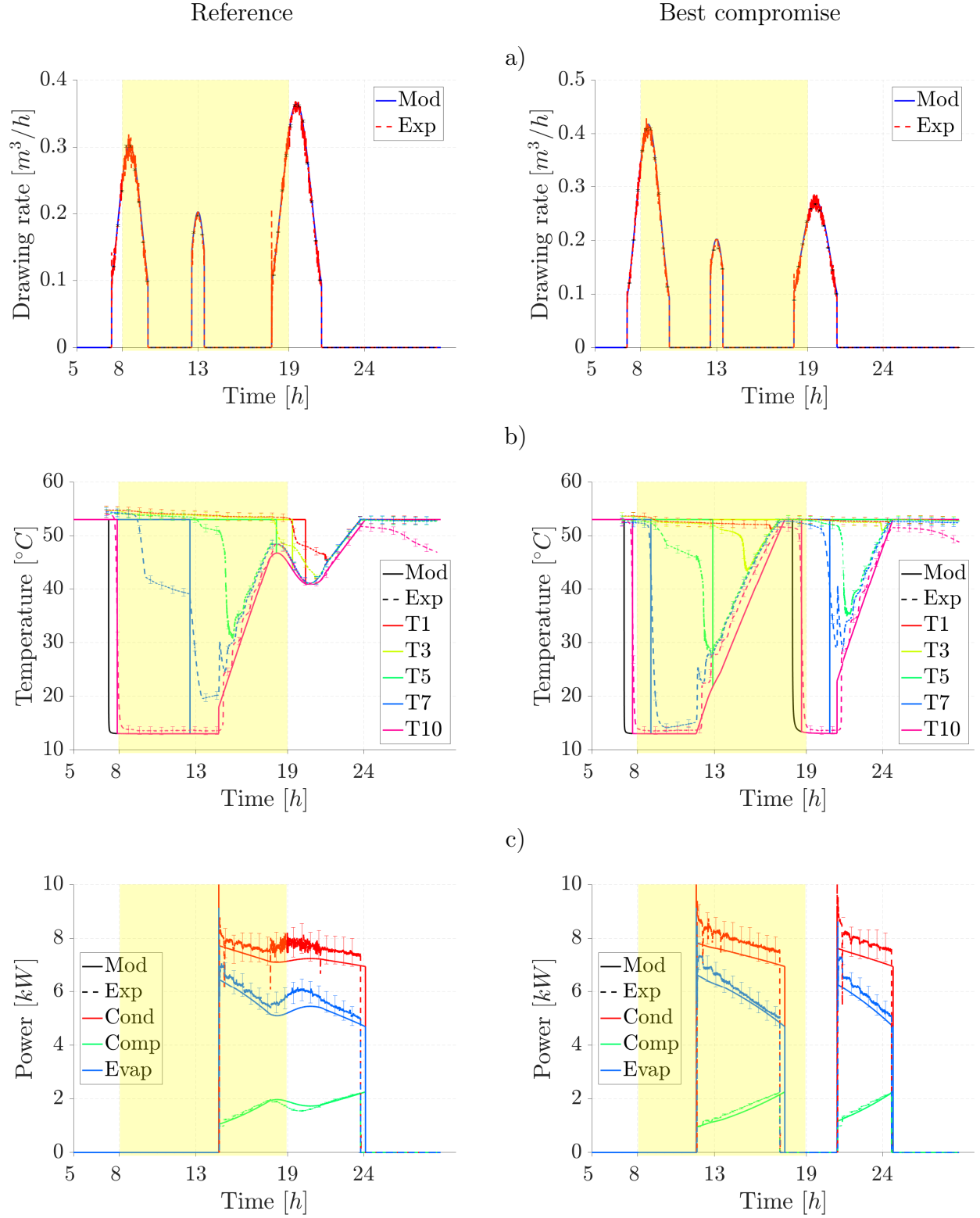


Figure 12: Evolution of the DHW demand profile a), temperatures b) and powers c) for the reference case (on the left) and for the optimized solution (on the right). The experimental profiles are presented by continuous curves and the numerical ones by dotted curves. The bars correspond to the uncertainties.

Figure 12 c), on the right, presents the variation in power over the day. The power of the heat pump is activated a first time at 12 h with an equivalent power compared to the reference case. However, the HP is disabled at 17.3 h because the tank is already filled with hot water. Then, the heat pump switches on in the evening during 3.5 h . The power produced by the HP decreases
465 with the time because the temperature in the storage is larger and therefore more electrical energy must be consumed from the compressor to produce less thermal energy from the condenser.

Table 8 shows the value of the objectives for the reference case. The experimental COP is 3.221, which represents a relative deviation of 2.3 % with the model. Indeed, the experimental produced
470 energy is 68.14 kWh and the consumed energy is 21.16 kWh which is composed of 15.90 kWh , 0.46 kWh and 4.80 kWh for the compressor, circulators and fan, respectively. Furthermore, the experimental E_{aux} is 11.63 kWh with a relative deviation of 8.5 %. In fact, the recovered energy by the PV collectors is 9.53 kWh which is splitted into 7.11 kWh , 0.22 kWh and 2.20 kWh for the compressor, circulators and fan, respectively. Similarly, for the optimized solution, the ex-
475 perimental COP is 3.444 with a relative deviation of 0.2 %, so the results are compatible with the numerical model. Moreover, the produced energy is 68.20 kWh and the energy consumption is 19.81 kWh . The experimental E_{aux} is 8.701 kWh with a relative deviation of 2.6 %, which is consistent with the numerical data. The recovered energy by the PV collectors is 11.10 kWh .

/		Objectives					Variables		
Names	COP^{num}	COP^{exp}	α	E_{aux}^{num}	E_{aux}^{exp}	α	Z_{sensor}^*	$V_{peak\ 1}^*$	Δh
Units	—	—	%	kWh	kWh	%	—	—	h
<i>Ref</i>	3.148	3.221	2.3	12.62	11.63	8.5	0.549	0.350	6.000
<i>Opt</i>	3.450	3.444	0.2	8.926	8.701	2.6	0.745	0.513	3.322

Table 8: Comparison of the numerical and experimental objectives for the reference case and for the optimized solution. The bold characters indicate that the heat pump is regulated from $V_{pic\ 1}^*$ or Δh .

480 The measurement uncertainty on the DHW demand profile increases when the flow rate is higher because this value is 0.5 %. Furthermore, the uncertainties on the DHW storage temperature are constant with a value of 0.71 $^{\circ}C$. The uncertainty of the compressor power is very small with a

value of about 0.01 kW and those of the evaporator and condenser powers are larger with values ranging from 0.3 kW to 0.5 kW . This variation is explained by the propagation of uncertainties
485 on the density, on the heat capacity and more specifically on the flow rate and on the temperature. The values of the numerical powers are included in the error bars, which allows to have a good reliability of the measurements.

As a result, the experimental and numerical results show relative differences of less than 10 %. The
490 experimental optimization procedure is confirmed because the objectives values are significantly improved, which has resulted in better regulation of the heat pump and the DHW demand profile.

5. Sensitivity study procedure

In this study, the sensitivity study is performed in three steps. Firstly, a sensitivity study with factorial plans, verifies that the solution obtained corresponds to the best compromise. Secondly,
495 a decision aid procedure is used to select the set of parameters that degrades the objectives most significantly compared to the optimal solution. Thirdly, the solutions of the factorial plans are carried out experimentally.

5.1. Sensitivity study

The sensitivity study is used to check if the solution selected by the optimization procedure corresponds to the optimal solution. Furthermore, the factorial plans determine the set of parameters that allows for the strongest degradation on the objectives from the best compromise. The minimum and maximum bounds are defined from the optimal solution X_{opt} and three factors $\sigma = (\sigma_1, \sigma_2, \sigma_3)$ which vary between 0 and ± 20 % with a step of ± 5 %. The expression of X_{min} and X_{max} are defined by:

$$\begin{cases} X_{min} &= X_{opt} (1 - \sigma) \\ X_{max} &= X_{opt} (1 + \sigma) \end{cases} \quad (29)$$

Figure 13 a) shows the solutions obtained by factorial plans. Many solutions are far away from the Pareto front because they significantly degrade the COP between 5 and 10 %. Figure 13 b) zooms on the Pareto front and on the optimal solution. None of the blue points are superimposed on the Pareto front so the application of the decision-making method illustrates that the selected optimal solution is verified.

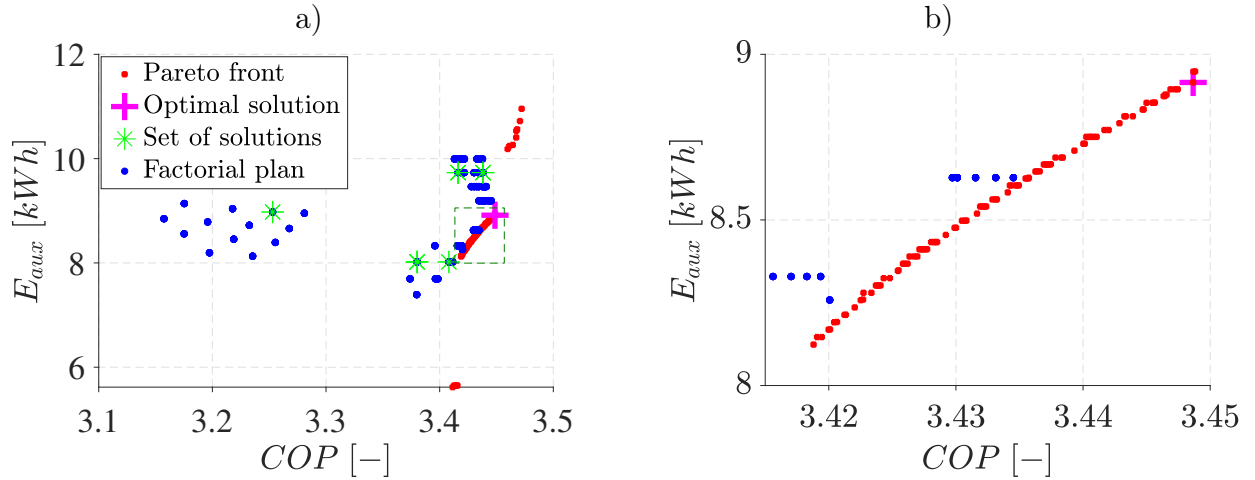


Figure 13: Solutions obtained by factorial plans a). The red dots are the Pareto front. The pink cross is the optimal solution. Zoom of the dotted part b).

5.2. Multi-criteria decision-making applied to sensitivity study

The TOPSIS decision-making method is applied to the sensitivity study in order to check if the solution obtained by the optimization process is the best compromise. The aim is to find the set of eight solutions that strongly degrades both objectives considering that the three factors can vary between 0 and ± 20 % compared to the optimal solution. The TOPSIS method shows that the value of the factor is equal to $\sigma_1 = \pm 20$ % for Z_{sensor}^* , $\sigma_2 = \pm 15$ % for V_{peak1}^* and $\sigma_3 = \pm 20$ %

for Δh .

$$\left\{ \begin{array}{lcl} Z_{sensor}^* & = & 0.745 \pm 20 \% = [0.549, 0.941] \\ V_{peak1}^* & = & 0.513 \pm 15 \% = [0.436, 0.590] \\ \Delta h & = & 3.322 \pm 20 \% = [2.637, 3.955] \end{array} \right. \quad (30)$$

Table 9 shows that the eight solutions have shown a strong degradation for the COP and the E_{aux} . Indeed, the solutions have a coefficient of performance smaller than 3.450 with relative deviations α varying between 0.4 and 5.7 %. Similarly, the solutions $n^\circ 1, 2, 5, 6, 8$ have an auxiliary energy larger than 8.926 kWh with a degradation of α between 0.7 and 9.0 %, and the other solutions
510 achieve an improvement of 10.3 % compared to the optimal solution.

Moreover, the value of the objectives of the second solution is identical to the first one. Indeed, the COP and the E_{aux} are equal to 3.418 and 9.732 kWh , respectively, while the value of Z_{sensor}^* of the solution $n^\circ 2$ increases by 0.4 compared to the $n^\circ 1$. In fact, the value of the objectives is unchanged because the system is not regulated from the sensor position but from the HP activa-
515 tion delay, so this variable has no influence on the two objectives. The same observation is noticed for the solutions $n^\circ 5$ and $n^\circ 6$ since the COP and the E_{aux} are equal to 3.437 and 9.732 kWh , respectively. In addition, the solutions $n^\circ 3$ and $n^\circ 7$ have the same value for the coefficient of performance and the auxiliary energy ($COP = 3.383$ and $E_{aux} = 8.005 kWh$) because the system is not controlled from the HP activation delay.

520

For the rest of this study, ten experimental tests are carried out to validate the optimization procedure. Two tests use the reference case and the optimized solution presented in table 7. The others eight tests correspond to factorial plans solutions given in table 9.

5.3. Experimental sensitivity procedure

525 The experimental tests are carried out based on the results obtained by the factorial plan presented in table 10. The DHW demand profile has an influence on the heat pump regulation, since the increase of V_{pic1}^* leads to a larger DHW consumption in the morning. In this case, the thermocline

/	Objectifs				Variables		
Nom	COP	α	E_{aux}	α	Z_{capt}^*	V_{pic1}^*	Δh
Unité	—	%	kWh	%	—	—	h
Opt	3.450	0.0	8.926	0.0	0.745	0.513	3.322
$PF\ n^{\circ}1$	3.418	0.9	9.732	9.0	0.549	0.436	2.637
$PF\ n^{\circ}2$	3.418	0.9	9.732	9.0	0.941	0.436	2.637
$PF\ n^{\circ}3$	3.383	1.9	8.005	10.3	0.549	0.590	2.637
$PF\ n^{\circ}4$	3.409	1.2	8.005	10.3	0.941	0.590	2.637
$PF\ n^{\circ}5$	3.437	0.4	9.732	9.0	0.549	0.436	3.955
$PF\ n^{\circ}6$	3.437	0.4	9.732	9.0	0.941	0.436	3.955
$PF\ n^{\circ}7$	3.383	1.9	8.005	10.3	0.549	0.590	3.955
$PF\ n^{\circ}8$	3.252	5.7	8.987	0.7	0.941	0.590	3.955

Table 9: Coordinates of factorial plans solutions. α corresponds to the relative deviations between the solutions of the factorial plans. The bold characters indicate that the heat pump is regulated from V_{pic1}^* or Δh . α is the relative deviation between the solutions of the factorial plans and the best compromise.

position increases and reaches the sensor position faster and therefore the heat pump is activated from Z_{capt}^* , which is the case of the solutions $n^{\circ} 3/7$.

530

The results show that the relative deviations are small because α is not larger than 10 % for all the solutions realized. These tests verify that the solutions $n^{\circ} 1/2$ do not have the same values for the objectives, compared to numerical data, but the regulation is effectively carried out from the activation delay. The same observation is noticed for the solutions $n^{\circ} 5/6$. The value of the objectives $n^{\circ} 3/7$ are very close, because the heat pump is regulated by the position of the sensor. Moreover, the model is based on a simplification of the physics, which may explain the differences between the solutions.

535

Table 11 shows the energy balance values, the coefficient of performance, the auxiliary energy and the associated uncertainties for the reference case. The uncertainty of the measurements is a cause of the differences between numerical and experimental data. Moreover, an uncertainty estimation is carried out to determine the dispersion of the measurements on the objective functions. The

540

/		Objectives					Variables		
Names	COP^{num}	COP^{exp}	α	E_{aux}^{num}	E_{aux}^{exp}	α	Z_{sensor}^*	V_{peak1}^*	Δh
Units	—	—	%	kWh	kWh	%	—	—	h
<i>Opt</i>	3.450	3.444	0.2	8.926	8.701	2.6	0.745	0.513	3.322
<i>PF n°1</i>	3.418	3.510	2.6	9.732	9.536	2.1	0.549	0.436	2.637
<i>PF n°2</i>	3.418	3.539	3.4	9.732	9.480	2.7	0.941	0.436	2.637
<i>PF n°3</i>	3.383	3.405	0.6	8.005	7.953	0.7	0.549	0.590	2.637
<i>PF n°4</i>	3.409	3.397	0.4	8.005	8.043	0.5	0.941	0.590	2.637
<i>PF n°5</i>	3.437	3.457	0.6	9.732	9.599	1.4	0.549	0.436	3.955
<i>PF n°6</i>	3.437	3.477	1.2	9.732	9.525	2.2	0.941	0.436	3.955
<i>PF n°7</i>	3.383	3.407	0.7	8.005	7.953	0.6	0.549	0.590	3.955
<i>PF n°8</i>	3.252	3.202	1.6	8.987	8.253	8.9	0.941	0.590	3.955

Table 10: Comparison of numerical and experimental objectives for factorial plans solutions. The bold characters indicate that the heat pump is regulated from V_{pic1}^* or Δh . α is the relative deviation between numerical and experimental data.

calculation shows that u_{COP} is 0.2 % and $u_{E_{aux}}$ is 0.5 %. For the coefficient of performance, the energy produced term contributes to 94 % of the uncertainties and the energy consumed term to 6 %. For the auxiliary energy, the consumed energy term is responsible for 59 % of the uncertainties and the PV energy term for 41 %. Therefore, the measurement uncertainties provide a good reliability of the experimental tests.

Name	Value	Uncertainty	Unit
E_{fan}	4.800	$2.450 * 10^{-4}$	kWh
E_{circ}	0.464	$4.012 * 10^{-5}$	kWh
E_{comp}	15.89	$4.012 * 10^{-3}$	kWh
E_{prod}	68.14	$4.071 * 10^{-2}$	kWh
E_{cons}	21.16	$4.208 * 10^{-3}$	kWh
$E_{prod_{PV}}$	9.530	$2.987 * 10^{-3}$	kWh
COP	3.221	$2.094 * 10^{-3}$	-
E_{aux}	11.63	$5.234 * 10^{-3}$	kWh

Table 11: Summary of measurement uncertainties for the reference case.

As a result, the relative deviations of the different solutions are small between the model and experimental data. The experimental sensitivity procedure is verified because the set of solutions in the factorial plans are dominated by the optimal solution, thus validating the optimization

methodology.

6. Conclusions and perspectives

In this study, a multi-criteria optimization methodology is applied to a DHW production system composed of a heat pump and a thermal storage. The two energy criteria are the coefficient of performance COP and the auxiliary energy E_{aux} . The three system parameters are the DHW demand shape and two regulation parameters that allow the HP to be switched on from the sensor position or from an activation delay. The DHW demand profile is composed of three Gaussian curves which represent the daily DHW consumption. The two physical constraints are to provide the DHW needs and to eliminate legionella. Moreover, two experimental constraints are also taken into account: (i) the tank is made of only ten sensors; (ii) this profile is truncated from a minimum flow rate since the experimental solenoid valve has a minimum sensibility of $0.1 \text{ m}^3 \cdot \text{h}^{-1}$. The results of the optimization procedure show that the optimal solution is obtained for a first peak volume of 0.513, a thermocline position of 0.745 and an activation delay of 3.322 h after the first consumption peak. This solution gives a $COP = 3.450$ and a $E_{aux} = 8.926 \text{ kWh}$, in this case, the heat pump operates to heat the DHW storage during the day, which is in adequacy with the production of the PV collectors. Furthermore, the experimental tests are carried out using an experimental test bench located in the IUSTI laboratory for the reference case and for the optimized solution. The optimization procedure is validated because the experiments has verified the improvement of the objectives. In addition, a sensitivity procedure is performed to determine the impact of parameter on the objectives. The values of the variation factors are $\sigma_1 = 20 \%$ for Z_{sensor}^* , $\sigma_2 = 15 \%$ for V_{peak1}^* and $\sigma_3 = 20 \%$ for Δh compared to the optimal solution. This set of parameters allows having the largest degradation of the COP and the E_{aux} compared to the optimal values. The solutions of factorial plans are performed experimentally and the results show that the relative deviations between the numerical and experimental solutions are small. Moreover, the DHW demand profile has an influence on the heat pump regulation because the thermocline position reaches the

sensor position more quickly. Finally, the results of the optimization methodology lead to a net improvement of the system effectiveness. Indeed, the optimal solution from the test has a gain on the coefficient of performance of 6.9 % and on the auxiliary energy of 25.2 % compared to the reference solution. Thus, the system produces more thermal energy than it consumes in electrical energy and uses less auxiliary energy to meet the DHW's demand thanks to a better regulation of the HP. Indeed, it is better to activate the heat pump after the first peak of DHW consumption to maximize the use of the solar energy and therefore minimize the auxiliary energy. Moreover, it is necessary that the storage tank is filled a first time during the day to meet the consumption of DHW in the evening, the storage must be refilled a second time in the night to meet the DHW needs the next day and to eliminate legionella. The deactivate of the heat pump during the third peak of DHW demand allows to minimize its operating time and thus to maximize the *COP*. Furthermore, it is recommended to use more hot water in the morning than in the evening to improve the performance of the system.

590

In future works, an experimental system and associated numerical modeling coupling domestic hot water and heating demands should be investigated. In this case, the heat pump regulation must be improved for winter, summer and inter-seasonal conditions and for different air changes in a collective building using a multi-objective optimization study.

595 **Acknowledgment**

The authors would like to thank Stéphane Launay who initiated the project.

References

- [1] World energy balances: Overview (2019 edition), <https://www.iea.org/> (2019).
- [2] E. Fuentes, L. Arce, J. Salom, A review of domestic hot water consumption profiles for application in systems and buildings energy performance analysis, Renewable and Sustainable Energy Reviews 81 (2018) 1530–1547. doi:<https://doi.org/10.1016/j.rser.2017.05.229>.
- [3] Technical and scientific center of the building (cstb), risk management of legionella development in domestic hot water networks, cstb technical guide, accessed 17 October 2019 (2012).
- [4] Risk management of legionella development in domestic hot water systems - deficiencies and recommendations, <https://docplayer.fr/261098-Guide-technique-maitrise-du-risque-de-developpement-des-legionelles-dans-les-re.html> (2012).
- [5] U. Jordan, K. Vajen, Influence of the dhw load profile on the fractional energy savings: A case study of a solar combi-system with trnsys simulations, Solar Energy 69 (2001) 197–208, eURO-SUN 2000 Selected Proceedings. doi:[https://doi.org/10.1016/S0038-092X\(00\)00154-7](https://doi.org/10.1016/S0038-092X(00)00154-7).
- [6] R. Araya, F. Bustos, J. Contreras, A. Fuentes, Life-cycle savings for a flat-plate solar water collector plant in chile, Renewable Energy 112 (2017) 365–377. doi:[10.1016/j.renene.2017.05.036](https://doi.org/10.1016/j.renene.2017.05.036).
- [7] M. L. Nicolson, M. J. Fell, G. M. Huebner, Consumer demand for time of use electricity tariffs: A systematized review of the empirical evidence, Renewable and Sustainable Energy Reviews 97 (2018) 276–289. doi:<https://doi.org/10.1016/j.rser.2018.08.040>.
URL <https://www.sciencedirect.com/science/article/pii/S1364032118306257>

- [8] A. Hepbasli, Y. Kalinci, A review of heat pump water heating systems, Renewable and Sustainable Energy Reviews 13 (6) (2009) 1211 – 1229. doi:<https://doi.org/10.1016/j.rser.2008.08.002>.
- [9] Ademe (2016). the domestic hot water, <https://expertises.ademe.fr/batiment/passer-a-laction/elements-dequipement/leau-chaude-sanitaire>, accessed 11 April 2022.
- [10] The dhw-hp revives the hot water, <https://media.xpair.com/pdf/eau-chaude-sanitaire/synthese-pacte-ecs-ademe.pdf>, accessed 11 April 2022.
- [11] S. Launay, B. Kadoch, O. Le Métayer, C. Parrado, Analysis strategy for multi-criteria optimization: Application to inter-seasonal solar heat storage for residential building needs, Energy 171 (2019) 419–439. doi:[10.1016/j.energy.2018.12.181](https://doi.org/10.1016/j.energy.2018.12.181).
- [12] J. Lu, Y. Tang, Z. Li, G. He, Solar heat pump configurations for water heating system in china, Applied Thermal Engineering 187 (2021) 116570. doi:<https://doi.org/10.1016/j.applthermaleng.2021.116570>.
- [13] F. Aguilar, S. Aledo, P. Quiles, Experimental study of the solar photovoltaic contribution for the domestic hot water production with heat pumps in dwellings, Applied Thermal Engineering 101 (2016) 379 – 389. doi:<https://doi.org/10.1016/j.applthermaleng.2016.01.127>.
- [14] A. Lapertot, M. Cuny, B. Kadoch, O. L. Metayer, Optimization of an earth-air heat exchanger combined with a heat recovery ventilation for residential building needs, Energy and Buildings (2021) 110702. doi:<https://doi.org/10.1016/j.enbuild.2020.110702>.
- [15] G. Segond, Study of thermal-hydraulic couplings of a thermal storage system under variable conditions: application to the domestic hot water supply system with the recovery of a low temperature heat source, Ph.D. thesis, PhD thesis supervised by Tadrist, Lounès and Launay, Stéphane, Aix-Marseille university (2015).

- [16] M. Baneshi, S. A. Bahreini, Impacts of hot water consumption pattern on optimum sizing and techno-economic aspects of residential hybrid solar water heating systems, Sustainable Energy Technologies and Assessments 30 (2018) 139 – 149. doi:<https://doi.org/10.1016/j.seta.2018.09.008>.
- [17] G. Mitsopoulos, E. Bellos, C. Tzivanidis, Parametric analysis and multi-objective optimization of a solar heating system for various building envelopes, Thermal Science and Engineering Progress 8 (2018) 307 – 317. doi:<https://doi.org/10.1016/j.tsep.2018.09.007>.
- [18] J. Assaf, B. Shabani, Multi-objective sizing optimisation of a solar-thermal system integrated with a solar-hydrogen combined heat and power system, using genetic algorithm, Energy Conversion and Management 164 (2018) 518 – 532. doi:<https://doi.org/10.1016/j.enconman.2018.03.026>.
- [19] R. Bornatico, M. Pfeiffer, A. Witzig, L. Guzzella, Optimal sizing of a solar thermal building installation using particle swarm optimization, Energy 41 (1) (2012) 31 – 37, 23rd International Conference on Efficiency, Cost, Optimization, Simulation and Environmental Impact of Energy Systems, ECOS 2010. doi:<https://doi.org/10.1016/j.energy.2011.05.026>.
- [20] E. Atasoy, B. Çetin, Özgür Bayer, Experiment-based optimization of an energy-efficient heat pump integrated water heater for household appliances, Energy 245 (2022) 123308. doi:<https://doi.org/10.1016/j.energy.2022.123308>.
URL <https://www.sciencedirect.com/science/article/pii/S0360544222002110>
- [21] J. Kline, F. A. McClintock, Describing uncertainties in single-sample experiments, Mechanical Engineering 75 (1953) 3–8.
- [22] Legionella risk management, french supreme council of public hygiene, https://solidarites-sante.gouv.fr/IMG/pdf/Rapport_du_CSHPF_de_novembre_2001_relatif_a_la_gestion_du_risque_lie_aux_legionelles.pdf (2001).

- [23] M. Ehrgott, Multicriteria Optimization, Springer-Verlag, Berlin, Heidelberg, 2005.
- [24] R. K. Arora, Optimization: Algorithms and applications, Hoboken : CRC Press, 2015. doi :
10.1201/b18469.
- 670 [25] J. Holland, Adaptation In Natural And Artificial Systems, University of Michigan Press, 1975.
- [26] K. Deb, A. Pratap, S. Agarwal, T. Meyarivan, A fast and elitist multiobjective genetic algorithm: NSGA-II, Evolutionary Computation, IEEE Transactions on 6 (2002) 182 – 197.
doi:10.1109/4235.996017.
- [27] G. H. Tzeng, J. J. Huang, Multiple attribute decision making: Methods and applications,
675 CRC Press, Taylor and Francis Group, A Chapman & Hall Book, Boca Raton, 2011. doi :
10.1201/b11032.
- [28] A. Saltelli, M. Ratto, T. Andres, F. Campolongo, J. Cariboni, D. Gatelli, M. Saisana, S. Tarantola, Global Sensitivity Analysis. The Primer, Vol. 304, John Wiley & Sons, 2008.
doi:10.1002/9780470725184.
- 680 [29] D. C. Montgomery, Design and analysis of experiments, 8th Edition, John Wiley & Sons, 2013.